Journal of Materials Chemistry B

Zwitterionic Liquid Crystalline Polythiophene as Antibiofouling Biomaterials

Journal:	*Journal of Materials Chemistry B*
Manuscript ID	TB-ART-09-2020-002264.R1
Article Type:	Paper
Date Submitted by the Author:	12-Nov-2020
Complete List of Authors:	Xu, Jinjia; Purdue University , ; National Institute for Materials Science, Xu, Jian; Purdue University Haesoo, Moon; Purdue University Sintim, Herman; Purdue University System, Chemistry Lee, Hyowon; Purdue University, Biomedical Engineering

ARTICLE

Zwitterionic Liquid Crystalline Polythiophene as Antibiofouling Biomaterials

Received 00th January 20xx,
Accepted 00th January 20xx

DOI: 10.1039/x0xx00000x

Jinjia Xu,*[a] Jian Xu,[a] Haesoo Moon,[a] Herman O. Sintim,[b] and Hyowon Lee*[a]

To address a key challenge of conjugated polymers in biomedical applications having poor antifouling properties that eventually lead to the failure and reduced lifetime of bioelectronics in the body, herein we describe the design, synthesis, and evaluation of our newly designed multifunctional zwitterionic liquid crystalline polymer **PCBTh-C8C10**, which is facilely synthesized using oxidative polymerization. The conjugated polythiophene backbones, multifunctional zwitterionic side chains, and a mesogenic unit are integrated into one segment. By DSC and POM characterization, we verify the introduction of 3,5-bis(2-octyl-1-dodecyloxy)benzene as a mesogenic unit into polythiophene backbone allows the formation of liquid crystalline mesophase of the resulting polymer. We also demonstrate that the **PCBTh-C8C10** coated surface exhibits good conductivity, stability, hydrophilicity, and remarkable antibiofouling properties against protein adsorption, cell growth, and bacteria attachment. This new zwitterionic liquid crystalline polymer having good antibiofouling features will be widely recognized as promising biomaterials that are applicable in implantable organic bioelectronics by inhibiting the foreign body response. The deep understanding on structure−property relationships of zwitterionic conjugated polymers has also been provided in this study.

1. Introduction

π-Conjugated liquid crystals (LCs) have attracted considerable attentions due to their ease of anisotropic interaction among mesogens, which generates distinctive behaviours that are difficult to achieve in crystalline materials.[1-4] LCs materials formed by π-conjugated molecules generally self-organize into an ordered supramolecular architecture, giving rise to the formation of various mesophases through strong π-π interactions between the poly-aromatic cores.[5-11] As such, π-conjugated liquid crystalline polymer materials are emerging as promising semiconducting soft materials because of their abilities to form one-dimensionally ordered nanostructures and have capabilities to reduce the grain boundary and structural defects for the formation of homogenous thin films, which are essential for the improvement of carrier-transport properties in device performance.[12-15] Designing side chains and/or new mesogenic units have recently emerged as an effective and general methods to access liquid crystalline mesophases of conjugated polymers, allowing greater control over crystalline morphologies and improving related device performance.[16-21] While promising potentials across a variety of applications are constantly being developed, many of them are struggling to maintain reliable functionality in complex *in vivo* environments over time due to the non-specific adsorption of biomacromolecules on biomedical device surfaces (i.e., biofouling) that reduce the sensitivity and performance of bioelectronic interfaces.[22-26] The zwitterionic polymers have been reported to be able to prevent non-specific bonding via the formation of a hydration layer to serve as a barrier between biomolecules and their surfaces.[27-42] Recently, our group reported zwitterionic conductive polymers that were demonstrated to have superior antibiofouling property, biocompatibility, and porosity.[28] Using LC mesophases to optimize morphologies of conjugated polymers is attractive as they allow for precise control over mesoscale features from the nano- to macroscale using simple and easy processing techniques.[42-45] However, there still remains challenges to create conjugated polymers that simultaneously exhibit liquid crystalline mesophases as well as good antibiofouling features due to limited molecular designs and synthetic difficulties.

[a] *Weldon School of Biomedical Engineering, Birck Nanotechnology Center, Center for Implantable Devices, Purdue University, West Lafayette, IN 47906, USA. Email: xu1267@purdue.edu and hwlee@purdue.edu*

[b] *Department of Chemistry, Center for Drug Discovery, Purdue Institute of Inflammation, Immunology and Infectious Disease, Purdue University, West Lafayette, IN 47906 USA.*

Electronic Supplementary Information (ESI) available: [details of any supplementary information available should be included here]. See DOI: 10.1039/x0xx00000x

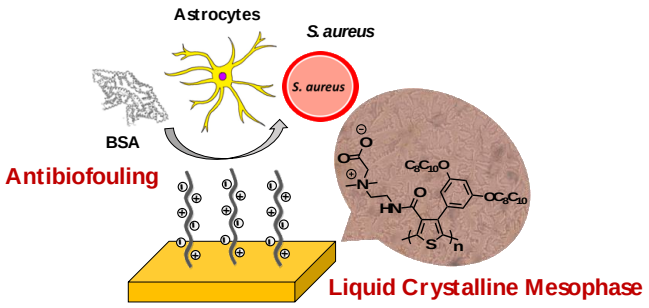

Scheme 1. The illustration of design and molecular structure of polymer **PCBTh-C8C10** in this study, which has superior antibiofouling properties against protein adsorption, cell growth, and bacteria attachment.

In this work, we report the design, synthesis, and characterization of newly designed zwitterionic liquid crystalline polymer **PCBTh-C8C10**, consisting of conjugated polythiophene backbones, multifunctional zwitterionic side chains, and a mesogenic unit that are integrated in one segment. Using DSC and POM measurements, we verified that the introduction of 3,5-bis(2-octyl-1-dodecyloxy)benzene as a mesogenic unit into polythiophene backbone allows the formation of liquid crystalline mesophase of resulting polymer. Furthermore, the zwitterionic side chain functionality makes **PCBTh-C8C10** exhibit remarkable antibiofouling properties against proteins adsorption, cells adhesion, and bacteria attachment while maintaining good conductivity. This newly developed zwitterionic liquid crystalline polymer **PCBTh-C8C10** can be used as multifunctional protective layers coated onto the surface of bioelectronic devices, thereby potentially prolonging the lifetime of implantable biomedical devices. The impact of such a structural change has on mesostructures as well as antibiofouling properties is studied herein.

2. Experimental Section

2.1. Raw Materials

1,1'-Carbonyldiimidazole (CDI), 4-Bromothiophene-3-carboxylic acid, N-hydroxysuccinimide (NHS) and tris(2-carboxyethyl)phosphine hydrochloride (TCEP) were purchased from Chem-Impex International (Wood Dale, IL, USA). Thermo initiator 2,2'-Azobis[2-(2-imidazolin-2-yl)propane]dihydrochloride (VA-044) was purchased from Wako Chemicals USA, Inc. (Richmond, VA, USA). Anhydrous tetrahydrofuran (THF), anhydrous chloroform, methanol, anhydrous dichloromethane, anhydrous toluene, anhydrous N,N-dimethylformamide, ethyl acetate, acetonitrile, cystaminedihydrochloride, N,N'-dimethylethylenediamine, ethyl bromoacetate, N-Bromosuccinimide (NBS), boron tribromide, triphenylphosphine, 2-octyl-1-dodecanol, anhydrous $FeCl_3$, tetrakis(triphenylphosphine)palladium(0), sodium carbonate, potassium carbonate, sodium hydroxide, glucose were purchased from Sigma-Aldrich (St. Louis, MO, USA). All chemicals were used as received without further purification. Milli-Q water (18.2 MW/cm, Burlington, MA) was used. Air and water sensitive synthetic manipulations were performed under an N_2 atmosphere using standard Schlenk techniques. Human cerebral cortex astrocytes, astrocyte medium, cell freezing medium, fetal bovine serum, astrocyte growth supplement, and penicillin/streptomycin solution were purchased from ScienCell Researh Laboratories (Carlsbad, CA). CellTracker™ green CMFDA dye, phosphate-buffered saline (PBS, 10X, pH 7.4), albumin from bovine serum fluorescein conjugate (FITC-BSA), Dulbecco's phosphate-buffered saline (no calcium, no magnesium) (DPBS), Poly-D-lysine, LIVE/DEAD BacLight Bacterial Viability Kit were purchased from ThermoFisher Scientific (Waltham, MA). Tryptic soy broth (TSB) was purchases from Becton Dickinson (Franklin Lakes, NJ). Diced microscope slides and cover glass from Fisher Scientific (Pittsburgh, PA) were used as glass substrate after cleaning by acetone and drying.

2.2. Instruments

The ^{1}H-NMR spectra were recorded on a JEOL ECS-500 (500 MHz) spectrometer by using tetramethylsilane (0 ppm for ^{1}H NMR) as an internal standard. The UV-vis absorption spectra were recorded on a JASCO V-670 spectrophotometer in a quartz cuvettes of 1 mm path length. The PerkinElmer LS 55 fluorescence spectrometer as used to collect the fluorescence emission spectra of polymers in solution and film states. The surface morphology was captured using Hitachi S-4800 Field Emission scanning electron microscope (SEM) with 5kV as accelerating voltage, and analysed using imageJ. Electrochemical analysis of polymers was performed using a SP-200 potentiostat (Bio-logic USA, LLC, Knoxville, TN, USA). The polymer thin-films were coated on the surface of the working electrode. All electrochemical experiments were performed in a conventional three electrode cell configuration in 1X PBS (pH 7.0) as the supporting electrolyte (50 mL for all experiments). A scan rate of 100 mV/s and sampling interval of 1 mV/s were used for cyclic voltammetry (CV). Differential scanning calorimetry (DSC) measurements were performed on a DSC Model TA Q-20 under flowing a nitrogen atmosphere. The sample was encapsulated in a sealed aluminium pan, and an identical empty pan was used as the reference. The DSC data were obtained during the second heating/cooling cycles at a scan rate of 10 °C/min in the temperature range of 0 °C to 150 °C. Polarizing optical microscope (POM) Nikon ECLIPSE E200 equipped with a Mettlar FP82HT hot stage was used for visual observations.

2.3. Preparation of polymer thin-film

The graft to method was employed to fabricate the thin-films of polymer. The polymers were dissolved in methanol at a concentration of 10 mg/mL, followed by depositing 100 µL of polymer methanol solution on a clean glass substrate. Then it was left undisturbed until solvent evaporated at room temperature. The samples were washed with PBS buffer solution five times and dried with filtered air prior to further characterizations.

2.4. Protein Adsorption Study

The antibiofouling performance of polymer-coated surfaces against protein was tested by comparing fluorescent intensity of respective samples incubated with BSA-FITC. Pristine samples, **PCBTh** coated, and **PCBTh-C8C10** coated cover glasses were incubated with BSA-FITC in 1X PBS solution of various concentrations in 6-well plates for 4 hours. Then, samples were gently rinsed with 1X PBS solution to remove unabsorbed protein before capturing images by using a fluorescence microscope (Axio Observer Z1, Carl Zeiss Microscopy, Jena, Germany) with a filter set 17 (excitation, BP 485/20, and emission BP 515-565, Carl Zeiss Microscopy, LLC). We used ImageJ to quantify the Image fluorescent intensities.

2.5. Cell Attachment

Here we chose astrocyte medium containing 500 mL of basal medium, 10 mL of fetal bovine serum (FBS, Cat. No. 0010), 5 mL of astrocyte growth supplement (AGS, Cat. No. 1852), and 5 mL of penicillin/streptomycin solution (P/S, Cat. No. 0503). Human cerebral cortex astrocytes were cryopreserved at passage one. Astrocytes were expanded and maintained per Sciencell's protocol. Astrocytes were cultured in 12-well, tissue culture-treated plates, with 1 x 10^5 cells seeded per well. These cultures were then incubated until confluent (48 h) in a humidified atmosphere with 5% CO_2 at 37°C. The medium was replaced one day after seeding. Cells were stained with CellTracker™ Green CMFDA. We replaced cell culture medium in each well with a 1:1000 ratio of dye to medium and incubated at 37°C for 30 min.

2.6. Bacterial Attachment and Biofilm Formation Array

The antibiofouling performance of polymer-coated surfaces against bacteria was examined by comparing the coverage of live and dead bacteria on respective samples incubated with *Staphylococcus aureus* (*S. aureus*). We used erythromycin-resistant *S. aureus* tagged with green fluorescent protein (GFP). Prior to each experiment, bacteria cultures were refreshed from stocks in 19:1:0.02 (v:v:v) TSB: 20% (w/v) glucose: erythromycin medium at 37°C for 12 h at 250 rpm. Then, bacteria cultures were diluted to 1/1000 into the same growth medium. In order to start the biofilm growth, 5 mL of the bacteria solution was then aliquoted to each sample, which was previously incubated in 5 mL of 1:9 (v:v) Poly-D-lysine: 1X PBS solution for 12 h at room temperature to improve bacteria attachment. After incubation at 37°C for 48 h at 50 rpm, 1.5 µL propidium iodide (PI) from bacterial viability kit was added to stain the dead bacteria. After the aspiration of bacteria solution and proper air drying, the biofilms were imaged using a confocal laser scanning microscope (ZEISS LSM 880, Carl Zeiss, Jena, Germany)). Z-stack images at 100x magnification were taken and analysed using Zeiss Zen software and MATLAB.

2.7. Statistical Analysis.

All values are reported as average ± standard deviation. Statistical analysis was performed using one-way analysis of variance (ANOVA) with Bonferroni correction using OriginPro 2018 software (Northampton, MA). A p-value lower than 0.05, 0.01, and 0.005 was denoted as *, **, and ***, respectively.

3. RESULTS AND DISCUSSIONS

3.1. Polymer Design, Synthesis, and Characterizations

As it has been reported, zwitterionic side chains attachment has been extensively studied and used as a soft segment in the development of novel biomaterials, which can effectively induce antibiofouling properties and increase the biocompatibility.[28] In our study, we designed and synthesized a multifunctional zwitterionic liquid crystalline polymer **PCBTh-C8C10**, which combines conjugated polythiophene backbones, zwitterionic side chains and a mesogenic unit 3,5-bis(2-octyl-1-dodecyloxy)benzene. As depicted in Scheme 1, we chose conjugated polythiophene as the conjugated backbone due to its good electrical conductivity, chemical stability, and unique electronic and optical properties.[46] The zwitterionic carboxybetaine was selected as the side chain because of its excellent antibiofouling property, good water solubility, and biocompatibility. The π-conjugated units attached with long alkoxy side chains have attached many interests because of their ability to self-assemble to form a mesophase.[1,2,5-8] It has been reported that the stacking behaviour of π-conjugated units provides opportunities for materials with one-dimensional transport processes, such as energy migration, electric conductivity, and photoconductivity. Because of 3,5-bis(2-octyl-1-dodecyloxy)benzene substituted at the 2-position on

thiophene, monomer **5** would possess good solubility, miserability, and the ability to self-organize into liquid crystalline mesophases that allows for precise control over desirable mesoscale features of resulting polymers. The synthetic routes for monomer **5** and polymer **PCBTh-C8C10** were summarized in Figure 1A. The compound **2** was synthesized from commercially available materials 4-bromothiophene-3-carboxylic acid according to modified literature procedures (Figure 1A).[28] Then compound **4** was synthesized by Williamson reaction of precursor **3**, which was prepared by demethylation reaction of 3,5-dimethoxyphenylboronic acid pinacol ester. Subsequent treatment of compound **4** with compound **2** under Suzuki coupling reaction conditions produced the zwitterionic side chain functionalized thiophene monomer **5**. **PCBTh-C8C10** polymer was then prepared by monomer **5** under oxidative polymerization in anhydrous chloroform using ferric chloride as the oxidant.[47] The resulting polymer **PCBTh-C8C10** exhibited as a yellow powder with good solubility in common organic solvents such as chloroform, methanol, and dichloromethane. The chemical structures of pure products were fully characterized and identified by using 1H and 13C nuclear magnetic resonance (NMR) spectroscopies (SI). The molecular structure of reference polymer **PCBTh** was also included in Figure 1B.

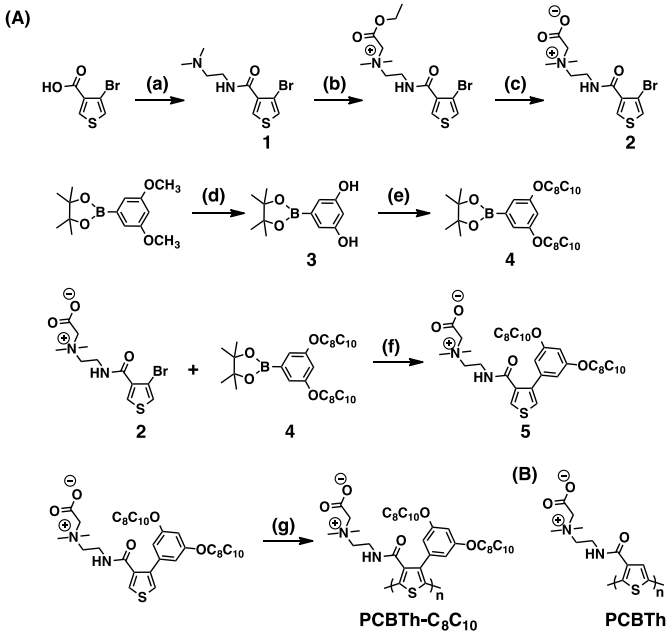

Figure 1. (A) Synthetic routes for monomer **5** and polymer **PCBTh-C8C10**. Reagents and conditions: (a) 1,1'-Carbonyldiimidazole (CDI), N,N'-dimethylethylenediamine, THF, 0°C, 24 h; (b) ethyl bromoacetate, 60°C, 2 days; (c) NaOH, H_2O; (d) BBr_3, DCM, 0°C; (e) $C_8C_{10}Br$, K_2CO_3, DMF, 90°C, 48 h; (f) $Pd(PPh_3)_4$, Na_2CO_3, toluene, H_2O, EtOH, reflux, overnight; (g) $FeCl_3$, $CHCl_3$, 24 h. (B) The molecular structure of reference polymer **PCBTh**.

3.2. Photophysical and Electrochemical Properties of Polymers

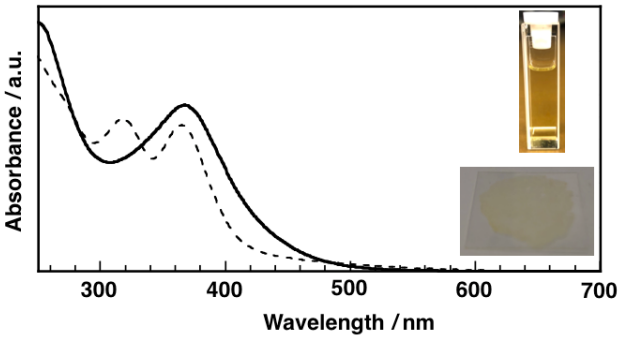

Figure 2. Normalized UV-vis absorption spectra of **PCBTh-C8C10** dissolved in methanol solution (solid lines) and in thin-film states as deposited (dash lines) at room temperature. Inset: photos of polymers dissolved in methanol solution and cast thin-film.

First, we systematically investigated the photophysical and electrochemical properties of **PCBTh-C8C10**. The UV-vis absorption spectra of polymers in solution and in thin solid film states were shown in Figure 2. Significantly, one intense absorption peak of **PCBTh-C8C10** was observed in the visible range with an absorption maximum at 367 nm (solid line) in methanol solution at 298 K. This characteristic absorption band can be reasonably assigned to $\pi-\pi^*$ transition of polythiophene backbone.[12] While one additional absorption peak of **PCBTh-C8C10** appeared in its thin-film state (dashed line), which undergoes 49 nm blue-shifted relative to the result from methanol solution spectra with a maximum absorption band at 318 nm. Optical bandgaps (E_g) between energy levels of highest occupied molecular orbital (E_{HOMO}) and the lowest unoccupied molecular orbital (E_{LUMO}) of **PCBTh-C8C10** estimated from absorption edge in the film state were 2.49 eV (Figure 2) as a comparison with the result of 3.59 eV from **PCBTh**.[28] The difference in absorption spectra and optical bandgaps between **PCBTh** and **PCBTh-C8C10** is probably responsible from the electron donating feature of 3,5-bis(2-octyl-1-dodecyloxy)benzene group. Similar to **PCBTh**, the fluorescence emission from **PCBTh-C8C10** was negligible in solution and film states (Figure S1). As newly established biomaterials, it is of great essence to have such low fluorescent background when it is regarded as biological matrices especially during the evaluation of its corresponding antibiofouling properties. Cyclic voltammetry (CV) measurements were used to investigate electrochemical properties of thin-film **PCBTh-C8C10** and **PCBTh** polymers (Figures 3 and S2), which showed comparable overall electrical conductivity relative to previously reported zwitterionic polymers.

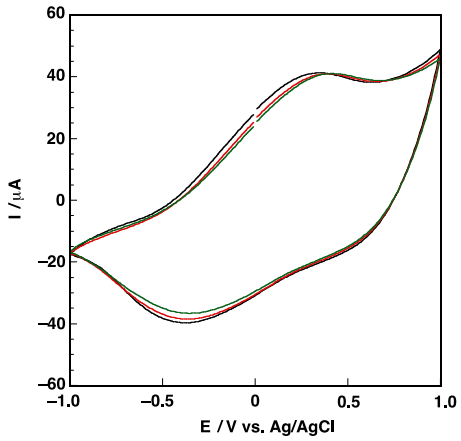

Figure 3. Cyclic voltammograms of **PCBTh-C8C10** thin-films with scan rate of 100 mV S^{-1} (First three cycles).

3.3. Liquid Crystalline Behaviour

The thermal phase behavior of **PCBTh-C8C10** was examined by differential scanning calorimetry (DSC), whereas the thermotropic liquid crystalline behavior was investigated by temperature-controlled polarizing optical microscopy (POM). Compared with the DSC result from **PCBTh** that has the amorphous property,[28] **PCBTh-C8C10** bearing a mesogenic unit at peripheral positions exhibited remarkable π-stacking to form ordered LC assemblies. As shown in Figure 4A, the DSC measurement of **PCBTh-C8C10** from 0 °C to 140 °C revealed the presence of phase transition from an isotropic liquid to a LC phase at 58 °C. The following phase transition was found at 29 °C, suggesting the crystallization behaviour of **PCBTh-C8C10** (Figure 4B). The POM images of **PCBTh-C8C10** exhibited fan-shaped textures at LC mesophases upon cooling from isotropic liquid at around 58 °C, which is the typical observation assigned for smectic LC assemblies (Figure 4C). Further heating over 98 °C led to disappearance of the birefringence, which corresponds to transition into isotropic liquid phase (Figure 4D). The observation of liquid crystalline texture indicated a smectic liquid crystalline structural formation, which is very similar to previously reported liquid crystalline polythiophene.[12] On the other hand, **PCBTh** did not show any distinct mesophases in both DSC and POM analyses, which suggested the importance of increased interaction between main chain and side mesogenic group attachments. The scanning electron microscopic observation also allows us to directly visualize the nanotexture of **PCBTh-C8C10** (Figure S3).

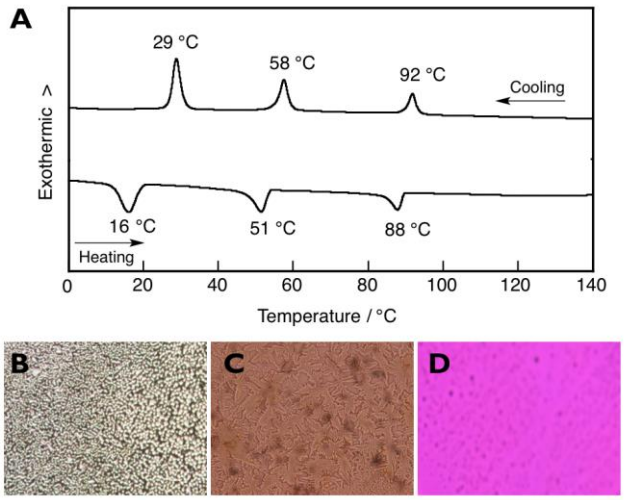

Figure 4. (A) Differential scanning calorimetry (DSC) trace of **PCBTh-C8C10** in the second sweeps with a heating and cooling scan rate of 10 °C/min; polarized optical microscope (POM) images of **PCBTh-C8C10** of thin films cast from its methanol solution under different temperatures: (B) at 29 °C, (C) at 59 °C and (D) at 95 °C.

3.4. Protein Adsorption Study

It has been widely known that protein adsorption on the surface of implantable biomedical devices plays an important role in initiating and regulating foreign body response, blood coagulation, and or inflammation, which will influence the functional performance and service lifetime of materials and devices.[48] It is environed that zwitterionic CB moieties can dramatically inhibit nonspecific protein adsorption and attachment on biomedical devices.

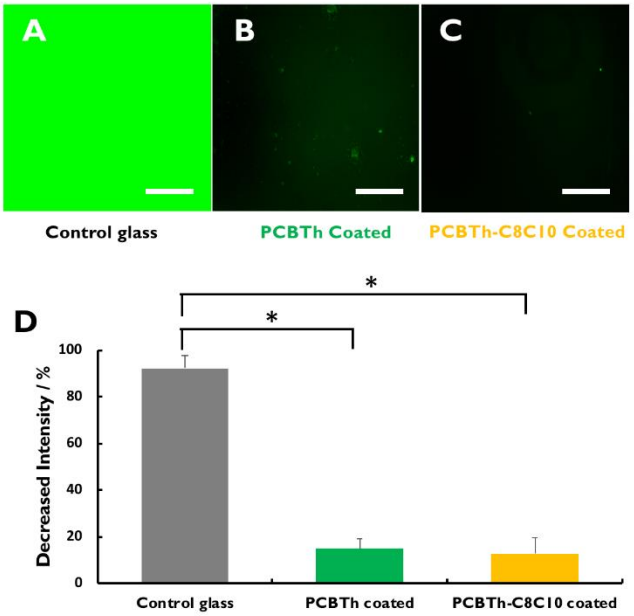

Figure 5. Fluorescence images of BSA-FITC (A) on pristine glass surface; (B) on **PCBTh** coated glass surface; and (C) on **PCBTh-C8C10** coated glass

surface; (scale bar: 200 μm) (D) comparison of decreased fluorescence intensity. *n* = 3 for each sample, calculated using one-way ANOVA with Bonferroni test.

Thus, we are motivated to test the protein adsorption on our **PCBTh-C8C10** polymer coated glass substrates. In order to demonstrate the anti-protein property of **PCBTh-C8C10** coated surfaces, a commonly used protein bovine serum albumin (BSA) was utilized for this study. As our previous finding[24] that the fluorescent intensity of absorbed BSA-FITC gradually increased and became saturated at a concentration of 6 mg/mL in PBS, to investigate the antibiofouling capability against BSA-FITC attachment, we incubated various testing samples in presence and absence of polymer coatings in BSA-FITC solution (6 mg/mL) for 4 h, and then evaluate the amount of adsorbed protein on pristine versus polymer-coated glass substrates. Under the fluorescence microscopic observation, we captured images of each sample and quantified the fluorescence intensity using imageJ. As shown in Figures 5A-C, the fluorescence intensity of **PCBTh-C8C10** coated surface was significantly reduced up to 87.2% compared to the pristine glass substrate. This decrease in protein adsorption was calculated to be a bit greater BSA-FITC reduction than that observed from **PCBTh** of 84.9%. The differences in fluorescence intensity between pristine glass substrate, **PCBTh** and **PCBTh-C8C10** coated surfaces were summarized in Figure 5D and Table 1. It is also worth noting that these results have good reproducibility and consistency. Similar to other reports claiming that strong hydration of zwitterionic materials provides effective protective layers to prevent biomacromolecules to interact with the materials surface, these results demonstrated that **PCBTh-C8C10** coated surface highly resist protein adsorption.

Table 1 The fluorescence intensity of the protein adhesion and the coverage of cells attachment on pristine and polymer-coated glass surfaces were measured and summarized (*n* = 3).

	Control glass	**PCBTh** coated	**PCBTh-C8C10** coated
Decreased Fluorescence intensity of BSA	92.3 ± 5.6	15.1 ± 4.1	12.8 ± 6.9
% of astrocytes coverage	23.6 ± 1.6	0.54 ± 0.2	0.006 ± 0.001

3.5. Cell Growth Study

For promising implantable biomedical devices, protein adsorption on their surfaces from blood can cause platelet, fibroblast, and astrocytes attachment.[49] Such kind of attachment easily leads to foreign body response, resulting in inflammation around implantable materials and biomedical devices. To further demonstrate the antibiofouling properties of polymer **PCBTh-C8C10**, cell adhesion experiments have been performed by using astrocytes, which are important immunological components of the central nervous system, participating in synaptic plasticity and information processing in the neuronal circuit. The interaction between astrocytes and neurons plays a crucial role in the development and progression of diverse neurological disorders. The astrocytes cultures were incubated to reach the confluency for 48h in a humidified atmosphere with 5% CO_2 at 37°C. The cell culture medium was replaced one day after seeding. After incubation for 48h, the control surface of uncoated glass substrate demonstrated a full coverage of 23.58% of astrocyte cells (Figure 6A). While minimal cells were found on the **PCBTh** coated glass substrate and completed inhabitation of cells adhesion was visualized on **PCBTh-C8C10** coated glass substrate (Figures 6B and 6C). The coverage of astrocyte cells on **PCBTh** and **PCBTh-C8C10** coated surfaces was evaluated to be 0.54% and 0.006%, respectively (Figure 6D and Table 1). These results supported our hypothesis that zwitterionic polymer coated surfaces can effectively resist adherent cell attachments as well. More in vivo studies of biocompatibility of **PCBTh-C8C10** is underway in our lab.

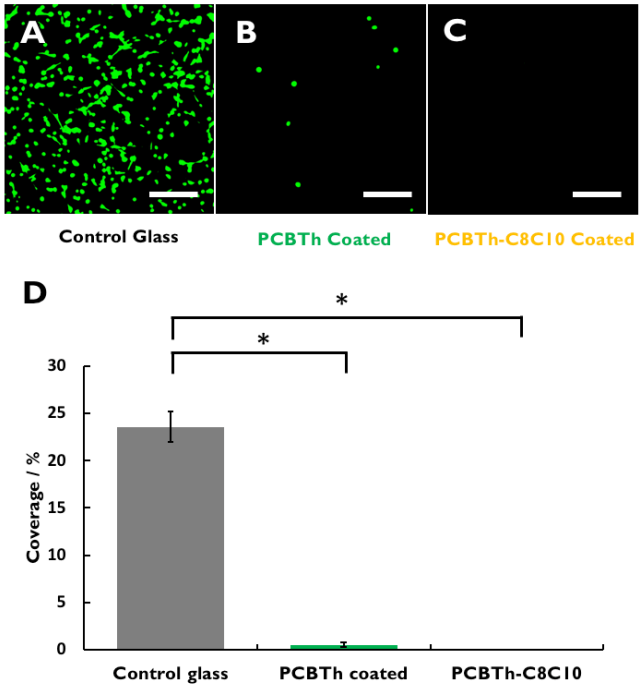

Figure 6. Representative fluorescence microscopy images of astrocytes cells attached on (A) pristine glass substrate; (B) **PCBTh**-coated glass surface; (C) **PCBTh-C8C10** coated glass surface after 48 h incubation in PBS buffer solution (scale bar: 200 μm); (D) Percentage of cell coverage on the surfaces with different treatments. *n* = 3 for each sample, calculated using one-way ANOVA with Bonferroni test.

3.6. Biofilm Formation in Vitro Arrays

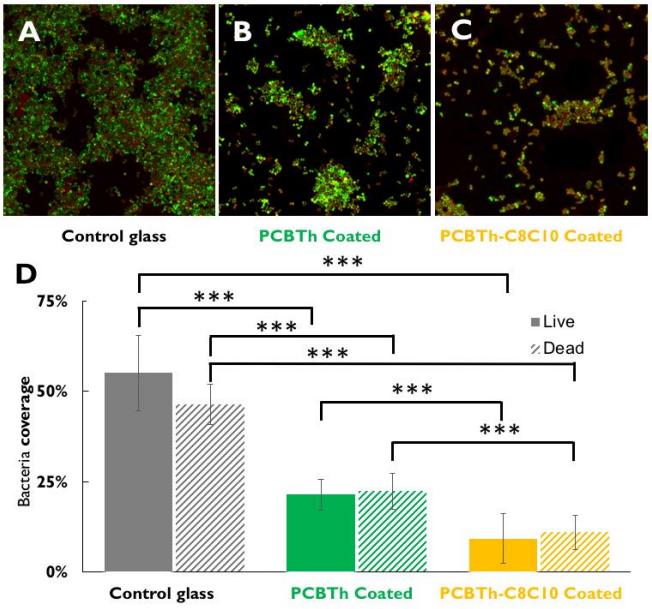

Figure 7. Representative confocal laser scanning microscopy (CLSM) images of *S. aureus* incubated on (A) pristine glass substrate; (B) **PCBTh**-coated glass surface; (C) **PCBTh-C8C10** coated glass surface for 48 h (scale bar: 20 μm); (D) quantitative percentages of bacteria coverage on these surfaces. *n* = 3 for each sample, calculated using one-way ANOVA with Bonferroni test.

Another major issue for implantable biomedical devices is the risk of infection that will likely cause the implant failure. The ability for *Staphylococcus aureus* (*S. aureus*) bacteria to adhere and proliferate on implantable biomedical devices is regarded as one of the major challenges in biomedical fields. As it is well known, the infections may be avoided by inhibiting initial adhesion of bacteria to the substrate surface, thus eliminating the possibility for an infection to occur on the surface of implants and diffuse to the surrounding areas. The new biomaterials with outstanding antibiofouling properties against bacterial attachment and biofilm formation are highly desirable. Thus, we also explored the antimicrobial properties of our polymer **PCBTh-C8C10** by using *S. aureus* as a model strain. The adherent bacteria coverage was quantified after incubation of glass samples with and without **PCBTh-C8C10** polymer coatings in *S. aureus* culture solution at 37°C for 48 h. In order to evaluate whether these polymers coated surface had the potential to inhibit *S. aureus* adhesion and growth, confocal laser scanning microscopy was used to quantify the coverage of live (green) and dead (red) bacteria on various glass samples following the incubation period. As shown in Figures 7B and 7C, our results suggest that the glass substrate coated with **PCBTh** can effectively inhibit *S. aureus* attachment during the 48 h incubation. Similarly, the **PCBTh-C8C10** coated surface exhibited a significant reduction in bacterial growth compared to the non-coated control glass substrate (Figures 7A-C). The amount of *S. aureus* on each surface was summarized in Figure 7D and Table 2. Our results showed that the zwitterionic liquid crystalline polymer **PCBTh-C8C10** coated surface possess a great capability to resist bacterial adhesion and colonization of biofilm-forming bacteria.

Table 2 The percentages of *S. aureus* coverage on pristine and polymer-coated surfaces were measured and summarized (*n* = 3).

Control glass		**PCBTh** coated		**PCBTh-C8C10** coated	
Live *S. aureus* (%)	Dead *S. aureus* (%)	Live *S. aureus* (%)	Dead *S. aureus* (%)	Live *S. aureus* (%)	Dead *S. aureus* (%)
55.15 ± 10.46	46.41 ± 5.69	21.40 ± 4.23	22.34 ± 4.95	9.13 ± 2.95	10.91 ± 3.66

4. Conclusions

In conclusion, a new zwitterionic polymer **PCBTh-C8C10**, consisting of conjugated polythiophene backbone, zwitterionic side chains and a mesogenic unit was designed and synthesized by oxidative polymerization. We found that the introduction of 3,5-bis(2-octyl-1-dodecyloxy)benzene mesogenic unit into the polythiophene backbone can facilitate the formation of thermotropic LC assemblies of resulting polymer. The characterization by DSC and POM revealed that the thermotropic highly-ordered mesophase was formed. Liquid crystalline mesophases arising from branched side chains in **PCBTh-C8C10** exhibited favourable control over macroscale structures, crystalline fraction, and molecular patterning, ultimately allowing for further utilization as novel biomaterials. In addition, we demonstrated that the **PCBTh-C8C10** polymer coated surface exhibited remarkable antibiofouling features against protein adsorption, cell adhesion as well as bacterial attachment. The study we present here will pave new avenues towards the development of semiconducting soft biomaterials and contribute to the rapid growing field of implantable bioelectronics.

Conflicts of interest

There are no conflicts to declare.

Acknowledgements

This work was supported in part by the National Science Foundation (United States) under Grants ECCS-1944480 and CNS-1726865, the Global Research Outreach program of Samsung Advanced Institute of Technology, and Eli Lilly Connected Care Program. The authors are grateful to Dr. Bryan Boudouris for allowing access to his laboratory during the polymer synthesis. The authors would also like to thank Dr. Lynne Taylor for the access to use polarizing optical microscope (POM). The authors would also like to thank Mr. Jim Nolan for his assistance with cell culture experiments.

Notes and references

1 S. Kumar, Taylor and Francis in Chemistry of Discotic Liquid Crystals: From Monomers to Polymers, CRC Press, Boca Raton, FL, 2011.
2 J. W. Goodby, P. J. Collings, T. Kato, C. Tschierske, H. Gleeson and P. Raynes in Handbook of Liquid Crystals 2nd edn, Wiley-VCH, Weinheim, Germany, 2014.
3 I. McCulloch, M. Heeney, C. Bailey, K. Genevicius, I. Macdonald, M. Shkunov, D. Sparrowe, S. Tierney, R. Wagner, W. Zhang, M. L. Chabinyc, R. J. Kline, M. D. McGehee and M. F. Toney, *Nat. Mater.*, 2006, **5**, 328–333.
4 H. Iino and J. Hanna, *Adv. Mater.*, 2011, **23**, 1748–1751.
5 S. Kumar, *Chem. Soc. Rev.*, 2006, **35**, 83–109.
6 S. Laschat, A. Baro, N. Steinke, F. Giesselmann, C. Hagele, G. Scalia, R. Judele, E. Kapatsina, S. Sauer, A. Schreivogel and M. Tosoni, *Angew. Chem. Int. Ed.*, 2007, **46**, 4832–4887.
7 S. Sergeyev, W. Pisula and Y. H. Geerts, *Chem. Soc. Rev.*, 2007, **36**, 1902–1929.
8 T. Wohrle, I. Wurzbach, J. Kirres, A. Kostidou, N. Kapernaum, J. Litterscheidt, J. C. Haenle, P. Staffeld, A. Baro, F. Giesselmann and S. Laschat, *Chem. Rev.*, 2016, **116**, 1139–1241.
9 Y. Sagara and T. Kato, *Angew. Chem. Int. Ed.*, 2008, **47**, 5175–5178.
10 H. Iino, T. Usui and J. Hanna, *Nat. Commun.*, 2015, **6**, 6828–6836.
11 S. Saito, S. Nobusue, E. Tsuzaka, C. Yuan, C. Mori, M. Hara, T. Seki, C. Camacho, S. Irle and S. Yamaguchi, *Nat. Commun.*, 2016, **7**, 12094–12101.
12 M. Watanabe, K. Tsuchiya, T. Shinnai and M. Kijima, *Macromolecules*, 2012, **45**, 1825–1832.
13 C. R. Bridges, M. J. Ford, B. C. Popere, G. C. Bazan and R. A. Segalman, *Macromolecules*, 2016, **49**, 7220–7229.
14 C. R. Bridges, M. J. Ford, G. C. Bazan and R. A. Segalman, *ACS Macro Lett*., 2017, **6**, 619–624.
15 C. R. Bridges, M. J. Ford, E. M. Thomas, C. Gomez, G. C. Bazan and R. A. Segalman, *Macromolecules*, 2018, **51**, 8597–8604.
16 J. Xu, *Polym. Chem.*, 2019, **10**, 6334–6341.
17 J. Xu, *New J. Chem.*, 2020, **44**, 3566–3569.
18 G. Lanzani, *Nature Mater.*, 2014, **13**, 775–776.
19 D. Fichou, Wiley-VCH, Weinheim, New York, 1999.
20 K. Tsuyoshi, O. Kazuchika, F. Tetsuya, and Y. Iwao, *J. Mater. Chem.*, 1994, **4**, 533–536.
21 D. Miyajima, F. Araoka, H. Takezoe, J. Kim, K. Kato, M. Takata and T. Aida, *Science*, 2012, **336**, 209–213.
22 M. R. Abidian and D. C. Martin, *Adv. Funct. Mater.*, 2009, **19**, 573-585.
23 R. A. Green, N. H. Lovell, G. G. Wallace and L. A. P. -Warren, *Biomaterials*, 2008, **29**, 3393–3399.
24 J. Xu, H. Moon, J. Xu, J. Lim, T. Fischer, H. A. McNally, H. O. Sintim and H. Lee, *ACS Appl. Mater. Interfaces*, 2020, **12**, 26893–26904.
25 J. Xu and H. Lee, *Chemosensors* 2020, **8**, 66–95.
26 H. Park, A. H. Raffiee, S. W. M. John, A. M. Ardekani and H. Lee, *Microsyst. Nanoeng.*, 2018, **4**, 35–47.
27 L. Zheng, H. S. Sundaram, Z. Wei, C. Li and Z. Yuan, *React. Funct. Polym.* 2017, **118**, 51–61.
28 J. Xu, J. Xu, H. Moon, H. O. Sintim and H. Lee, *ACS Appl. Polym. Mater.*, 2020, **2**, 528–536.
29 L. Zhang, Z. Cao, T. Bai, L. Carr, J.-R.-E. Menye, C. Irvin, B. D. Ratner and S. Jiang. *Nat. Biotechnol.*, 2013, **31**, 553–557.
30 X. Lin, X.; P. Jain, K. Wu, D. Hong, H.-C. Hung, M. B. O'Kelly, B. Li, P. Zhang, Z. Yuan and S. Jiang, *Laungmuir*, 2019, **35**, 1544–1551.
31 B. Cao, Q. Tang, L. L. Li, C. J. Lee, H. Wang, Y. Q. Zhang, H. Castaneda and G. Cheng, *Chem. Sci.*, 2015, **6**, 782–788.
32 B. Cao, C.-J. Lee, Z. Zeng, F. Cheng, F. Xu, H. Cong and G. Cheng, *Chem. Sci.*, 2016, **7**, 1976–1981.
33 B. Cao, L. L. Li, H. Y. Wu, T. Qiong, B. B. Sun, H. Dong, J. Zhe and G. Cheng, *Chem. Commun.,* 2014, **50**, 3234–3237.
34 H. Wang, Y. Hu, D. Lynch, M. Young, S. Li, H. Cong, F.-J. Xu and G. Cheng, *ACS Appl. Mater. Interfaces*, 2018, **10**, 37609–37617.
35 Y. N. Chou, F. Sun, H. C. Hung, P. Jain, A. Sinclair, P. Zhang, T. Bai, Y. Chang, T. C. Wen and Q. Yu, *Acta Biomater.*, 2016, **40**, 31–37.
36 Y. Hu, B. Liang, L. Fang, G. Ma, G. Yang, Q. Zhu, S. Chen and X. Ye, *Langmuir* 2016, **32**, 11763–11770.
37 H. Wu, C. J. Lee, H. Wang, Y. Hu, M. Young, Y. Han, F.J. Xu, H. Cong and G. Cheng, *Chem. Sci.*, 2018, **9**, 2540–2546.
38 J. Ladd, Z. Zhang, S. Chen, J. C. Hower and S. Jiang, *Biomacromolecules* 2008, **9**, 1357–1361.
39 S. Y. Lee, Y. Lee, P. LeThi, D. H. Oh and K. D. Park, *Biomater. Res.* 2018, **22**, 3–10.
40 L. Mi and S. Jiang, *Angew Chem. Int. Ed.*, 2014, **53**, 1746−1754.
41 S. Chen, J. Zheng, L. Li and S. Jiang, *J. Am. Chem. Soc.*, 2005, **127**, 14473−14478.
42 C. M. E. Tan, G. V. Dizon, S.-H. Chen, A. Venault, Y.-N. Chou, L. Tayo and Y. J. Chang, *J. Mater. Chem. B*, 2020, doi.org/10.1039/D0TB01478H.
43 M. C.-Valles, A. M.-Bueno, R. Gimenez, T. Sierra and M. B. Ros, *J. Mater. Chem. C*, 2019, **7**, 14454–14470.

44 C. R. Snyder, R. J. Kline, D. M. Delongchamp, R. C. Nieuwendaal, L. J. Richter, M. Heeney and I. McCulloch, *J. Polym. Sci. B Polym. Phys.*, 2015, **53**, 1641–1653

45 C. Tschierske, *Chem. Soc. Rev.*, 2007, **36**, 1930–1970.

46 S. Das, D. P. Chatterjee, R. Ghosh and A. K. Nandi, *RSC Adv.*, 2015, **5**, 20160–20177.

47 X. Pang, P. Imin, I. Zhitomirsky and A. Adronov, *Macromolecules*, 2010, **43**, 10376-10381.

48 J. N. Lockhart, T. J. Spoonmore, M. W. McCurdy, B. R. Rogers, S. A. Guelcher and E. Harth, *ACS Appl. Mater. Interfaces*, 2018, **10**, 4050–4056.

49 Y.-B. Sun, H. Zhao, D.-L. Mu, W. Zhang, J. Cui, L. Wu, A. Alam, D.-X. Wang and D. Ma, *Cell Death and Disease*, **2019**, *10*, 167–180.

ARTICLE

Table of Contents (TOC) graphic